nature climate change

ARTICLES

https://doi.org/10.1038/s41558-022-01374-w

Check for updates

Future reversal of warming-enhanced vegetation productivity in the Northern Hemisphere

Yichen Zhang[1], Shilong Piao[1,2] ✉, Yan Sun[3], Brendan M. Rogers[4], Xiangyi Li[1], Xu Lian[1], Zhihua Liu[5], Anping Chen[6] and Josep Peñuelas[7,8]

Climatic warming has greatly increased vegetation productivity in the extratropical Northern Hemisphere since the 1980s, but how long this positive relationship will continue remains unknown. Here we show changes in the effect of warming on Northern Hemisphere summer gross primary productivity for 2001–2100 using Earth system model outputs. The correlation between summer gross primary productivity and temperature decreases in temperate and boreal regions by the late twenty-first century, generally becoming significantly negative before 2070 in regions <60° N, though Arctic gross primary productivity continues to increase with further summer warming. The time when the correlation becomes negative is generally later than the time when summer temperature exceeds the optimal temperature for vegetation productivity, suggesting partial mitigation of the negative vegetation impacts of future warming with photosynthetic thermal acclimation. Our findings indicate that vegetation productivity could be impaired by climate change in the twenty-first century, which could negatively impact the global land carbon sink.

The terrestrial biosphere is a major carbon (C) sink that offsets about one-third of anthropogenic CO_2 emissions[1]. Approximately 40% of this global terrestrial C sink has been attributed to the extratropical Northern Hemisphere (NH; >23.5° N), which thus plays a critical role in mitigating global warming[2,3]. This large NH terrestrial C sink is primarily caused by higher vegetation gross primary productivity (GPP) under warming and rising atmospheric CO_2 concentrations[4–6]. However, how long the predicted further warming[7] will continue to increase extratropical NH productivity remains uncertain[8]. Recent studies from tree-ring records[9,10], satellite observations and simulated vegetation proxies[8,11,12] indicate a weakening or even negative temperature control on northern ecosystem productivity since the 1980s. These multiple lines of evidence suggest a potential reversal of warming-induced productivity increases in northern ecosystems that are supposedly thermally limited[13]. Exploring the threshold and timing at which GPP begins to respond negatively to summer warming in different regions and ecosystems and analysing the underlying causes is therefore critically important to deepen our understanding of the terrestrial C balance under a warming climate.

Summer is the peak season for plant photosynthesis in northern ecosystems and summer temperatures will probably exceed optimal thresholds for plant growth under climate change[8,14]. Using model outputs of ecosystem productivity for 2000–2100, we investigate how future summer (June–August) warming could affect ecosystem GPP across the extratropical NH and when summer warming could shift from having a positive to a negative impact on ecosystem GPP (Methods). We focus on summer warming because: (1) rising temperatures in summer have a direct metabolic impact on ecosystem productivity, particularly as current temperatures in most of the NH are still lower than the photosynthetic temperature optima[15,16], unlike in spring and autumn when warming mostly indirectly increases ecosystem productivity by extending the growing season[17–19]; and (2) photosynthetic activity in summer contributes to the largest decrease in atmospheric CO_2 concentrations within a year and thus to the interannual variability of annual productivity and the terrestrial C sink[20].

We first investigated the temporal change of the effect of summer warming on GPP across the extratropical NH in the future based on outputs from eight Earth system models (ESMs) participating in simulations of the Coupled Model Intercomparison Project Phase 6 (CMIP6)[21]. These eight models performed relatively well when evaluated using FLUXCOM GPP data and climatic data from Climatic Research Unit/National Centers for Environmental Protection (CRU/NCEP; Methods). We then assessed the timing at which summer warming begins to negatively affect GPP under different climate scenarios based on shared socioeconomic pathways (SSPs). Finally, we derived a satellite-based optimal temperature for vegetation productivity and coupled this to future temperature projections from the ESMs to investigate the observation-driven timing of photosynthetic downregulation under future warming.

Change in partial correlation between GPP and temperature

Figure 1a,b shows spatial patterns of multi-model mean correlations between summer GPP and temperature ($R_{GPP-Temp}$) for the end of this century (2081–2100) under SSP2-4.5 (intermediate emissions) and SSP5-8.5 (high emissions), respectively (Methods). These correlations remain positive by 2081–2100 under SSP2-4.5 for regions >60° N but become negative at lower latitudes (<45° N; Fig. 1a) of the extratropical NH, such as central and western North America, Europe and southern Russia, which could be attributed to water

[1]Sino-French Institute for Earth System Science, College of Urban and Environmental Sciences, Peking University, Beijing, China. [2]State Key Laboratory of Tibetan Plateau Earth System, Resources and Environment, Institute of Tibetan Plateau Research, Chinese Academy of Sciences, Beijing, China. [3]College of Marine Life Sciences, Ocean University of China, Qingdao, China. [4]Woodwell Climate Research Center, Falmouth, MA, USA. [5]CAS Key Laboratory of Forest Ecology and Management, Institute of Applied Ecology, Chinese Academy of Sciences, Shenyang, China. [6]Department of Biology and Graduate Degree Program in Ecology, Colorado State University, Fort Collins, CO, USA. [7]CREAF, Cerdanyola del Valles, Barcelona, Spain. [8]CSIC, Global Ecology Unit CREAF-CSIC-UAB, Barcelona, Spain. ✉e-mail: slpiao@pku.edu.cn

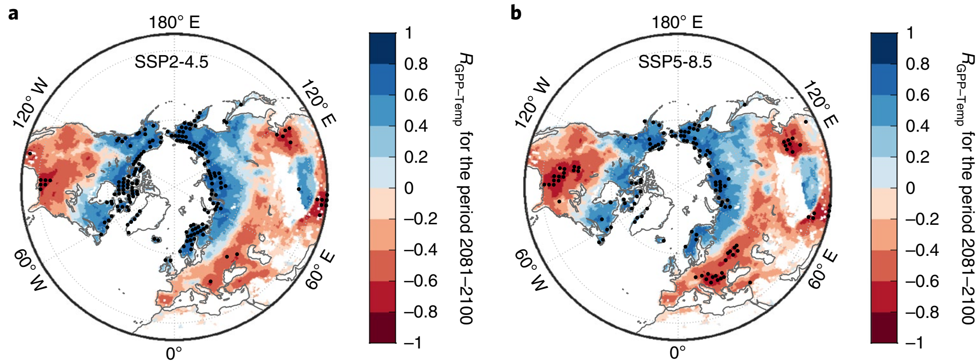

Fig. 1 | Spatial pattern of the partial correlation between summer GPP and temperature ($R_{GPP-Temp}$). a,b Multi-model averaged $R_{GPP-Temp}$ calculated using the eight CMIP6 ESMs for 2081–2100 under SSP2-4.5 (**a**) and SSP5-8.5 (**b**). Black dots indicate grid cells with significant multi-model mean $R_{GPP-Temp}$ ($P<0.05$).

deficits induced by warming (Supplementary Fig. 1). $R_{GPP-Temp}$, however, is mostly insignificantly positive on the Tibetan Plateau (mostly <45° N), probably because its mean summer temperature is lower than in other regions of similar latitudes (Supplementary Fig. 2). The spatial pattern of $R_{GPP-Temp}$ in 2081–2100 under SSP2-4.5 is notably similar to that of the first two decades of this century (2001–2020), which is also confirmed using satellite-based GPP proxies and CRU/NCEP temperatures (Supplementary Fig. 3). However, $R_{GPP-Temp}$ is lower in 2081–2100 than 2001–2020 across most regions, particularly in western Europe, eastern Siberia, the Tibetan Plateau and northwestern and northeastern North America (Supplementary Fig. 4a,b). The positive effect of warming on summer vegetation productivity decreases in northern and high-altitude regions and the negative effect of warming increases at lower latitudes, even under the intermediate emission scenario (Supplementary Fig. 4c,d).

$R_{GPP-Temp}$ in 2081–2100 has a similar latitudinal zonation pattern under SSP5-8.5 (Fig. 1b). The deterioration of summer GPP induced by warming under such a high-emission scenario, however, is more severe across Europe and especially central North America, where $R_{GPP-Temp}$ is significantly negative across larger areas. The area with a significantly positive $R_{GPP-Temp}$ is also less extensive under SSP5-8.5 (11.1% of NH pixels) than under SSP2-4.5 (16.2% of NH pixels), even for regions that have more positive than negative $R_{GPP-Temp}$ values, such as northern North America (23.5% of pixels under SSP2-4.5 versus 15.5% under SSP5-8.5). $R_{GPP-Temp}$ is also projected to decrease more at high latitudes (>45° N) under SSP5-8.5 (−0.12 under SSP5-8.5 versus −0.05 under SSP2-4.5) for 2020–2100. The correlation between summer GPP and temperature generally tends to decrease (including more negative values) widely in temperate and boreal regions by the late twenty-first century, which is consistent with the expectation that plants will suffer from increasing photosynthetic inhibition induced by warming in the future. These findings indicate that northern ecosystems will be more vulnerable to future climate change, with more frequent and longer summer heatwaves and higher average summer temperatures[22].

Reversal of warming-enhanced vegetation productivity

We next investigated the timing at which significantly negative summer $R_{GPP-Temp}$ ($t_{negative}$) first occurs (Methods). Results from the eight ESMs suggested that multi-model mean $t_{negative}$ is progressively delayed from the mid-low latitudes (~2030–2040) to the high latitudes (>2090) for SSP2-4.5 (Fig. 2a), in accordance with the latitudinal zonation of $R_{GPP-Temp}$ (Fig. 1). About 48% of the northern vegetated land will experience an emergent decrease in GPP induced by warming by 2060, and $R_{GPP-Temp}$ is positive only in regions >50° N (for example, the Labrador Plateau, northeastern coastal North America and northwestern coastal Asia) and the Tibetan Plateau. This ratio will rise to 78% by the end of this century, and $R_{GPP-Temp}$ is positive only in the Arctic, northeastern coastal North America, northeastern Siberia and part of the Labrador Plateau. SSP5-8.5 has similar spatial patterns of multi-model mean $t_{negative}$ (Fig. 2b). More than 80% of northern land, however, is projected to begin to respond negatively to temperature by the end of this century compared with SSP2-4.5.

Despite the general trend of the progressively delayed $t_{negative}$ from low to high latitudes, there is a substantial cross-model spread in the spatial patterns of $t_{negative}$ (Supplementary Figs. 5 and 6). Under the worst-case scenario (defined as the earliest 25th percentile of $t_{negative}$ by the eight ESMs), $t_{negative}$ is earlier than 2030 for most temperate regions at latitudes <50° N under both SSP2-4.5 and SSP5-8.5 (Fig. 2c,d). Under the best-case scenario (defined as the latest 25th percentile of $t_{negative}$ by the eight ESMs), $t_{negative}$ is only earlier than 2030 in a much smaller proportion of the land (Fig. 2e,f), in some lower-latitude regions such as east-central North America, northern China and parts of Europe and western Asia. The probability of a negative response of ecosystem productivity to warming in the coming decade is thus high for these regions. A positive $R_{GPP-Temp}$ continues to the end of this century for cold regions such as the Arctic, its surrounding area and the Tibetan Plateau, even in the worst-case scenario under both SSP2-4.5 and SSP5-8.5 (Fig. 2c,d).

Timing of temperature over optimal-productivity requirement

Finally, to gain insights into the relationship between the theoretical inflection point for photosynthesis and the emergence of the negative effects of warming simulated by the ESMs, we estimated the timing (t_{exceed}) when model-projected summer temperatures first exceed the optimal temperatures for vegetation productivity (T_{opt}) derived from satellite observations (Methods). Under both SSP scenarios, there was strong agreement across all ensemble ESMs on t_{exceed} (Supplementary Figs. 7 and 8), indicating high consistency in the ESM projections of future temperature changes. North America and Eurasia have different spatial patterns of multi-model mean t_{exceed} calculated by the eight ESMs under both SSP2-4.5 and SSP5-8.5 (Fig. 3a,b). For example, t_{exceed} in North America follows a latitudinal pattern for most of the land <45° N before 2030, and t_{exceed} at some higher latitudes occurs between 2050 and 2070. In Eurasia, however, t_{exceed} follows an east–west gradient, being earlier (before 2030) in western Eurasia (including Europe and central Siberia) than eastern Eurasia (mostly 2050–2070). This earlier t_{exceed} in western than in eastern Eurasia is probably due to the difference in their summer temperatures rather than the difference in the rates of future warming. Current summer temperatures are higher in

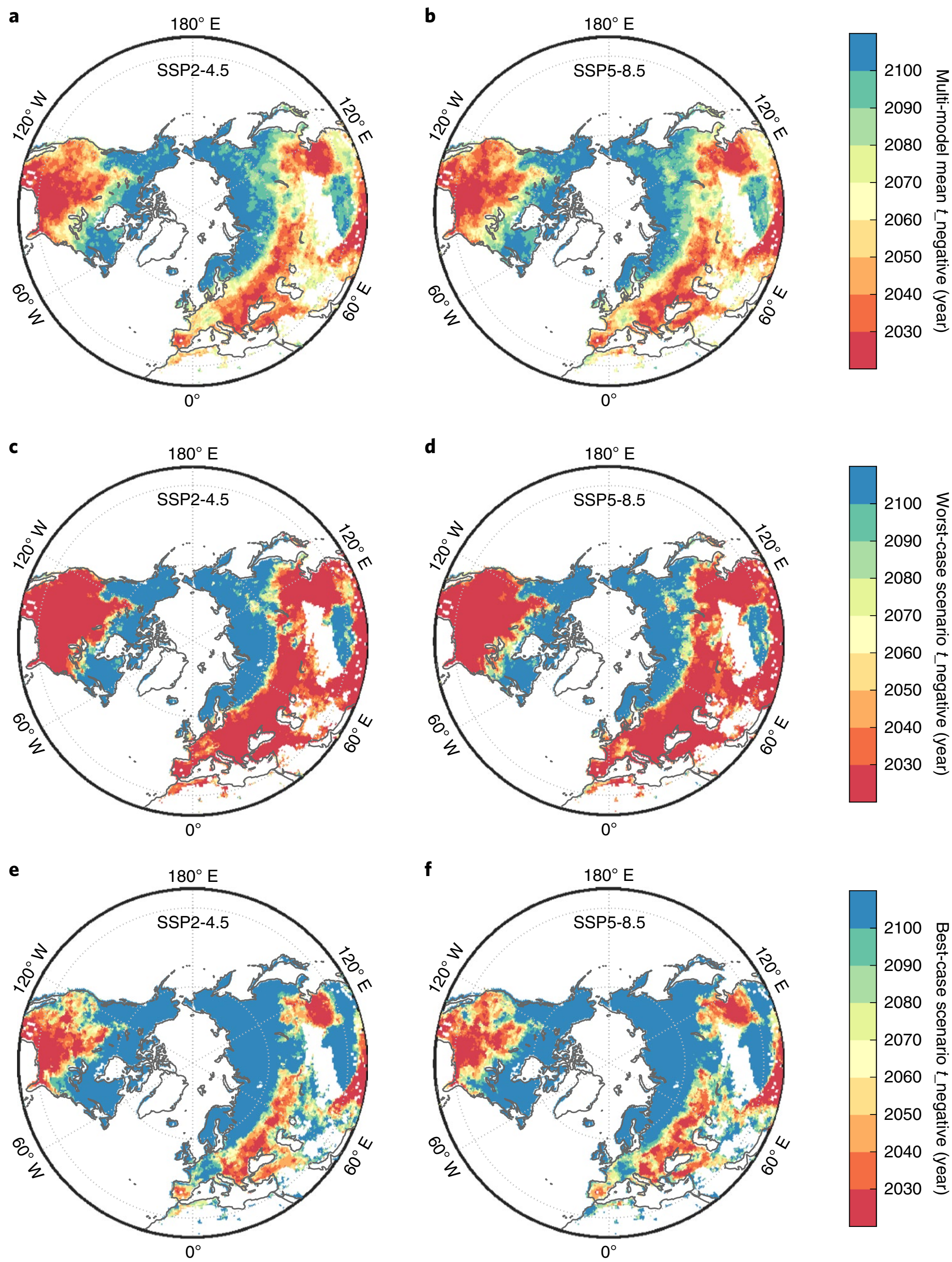

Fig. 2 | Spatiotemporal pattern of the emergent time of significantly negative $R_{GPP\text{-}Temp}$ ($t_{negative}$) during the twenty-first century. a,b, Multi-model averaged $t_{negative}$ under SSP2-4.5 (**a**) and SSP5-8.5 (**b**), defined as the time when $R_{GPP\text{-}Temp}$ first becomes significantly negative ($P < 0.05$). **c,d**, The worst-case scenario of multi-model $t_{negative}$ under SSP2-4.5 (**c**) and SSP5-8.5 (**d**), defined as the earliest 25th percentile across the eight models. **e,f**, The best-case scenario of multi-model $t_{negative}$ under SSP2-4.5 (**e**) and SSP5-8.5 (**f**), defined as the latest 25th percentile across the eight models.

western compared with eastern Eurasia (Supplementary Fig. 9b) and both regions have similar rates of future summer warming according to the ESMs (Supplementary Fig. 9c,d). T_{opt} is slightly higher in western than eastern Eurasia (Supplementary Fig. 9a), but the difference in T_{opt} between the two regions is much smaller than the difference in summer temperatures. The 'safety line' (the difference between T_{opt} and summer temperature) is accordingly lower in western than eastern Eurasia.

The worst- and best-case scenarios have similar spatial patterns of t_{exceed}. Under the best-case scenario (the latest 25th percentile of t_{exceed} projected by the eight models; Fig. 3e), t_{exceed} is earlier than 2030 under SSP2-4.5 in >67% of the extratropical NH, including western Eurasia and temperate North America, suggesting a very limited 'safety line' of vegetation productivity under the current level of warming. Under the best-case scenario, $t_{negative}$ is only projected to be later than 2080 under SSP2-4.5 in a few sporadic areas of northern North America and eastern Eurasia. For these regions, t_{exceed} could still occur as early as between 2050 and 2070 in the worst-case scenario (the earliest 25th percentile of t_{exceed} projected by the eight models; Fig. 3c). These results indicated that the entire extratropical NH may exceed its optimal temperature for productivity in the twenty-first century.

Discussion

We investigated the timing at which warming shifts from increasing to decreasing ecosystem productivity. We derived $t_{negative}$ based

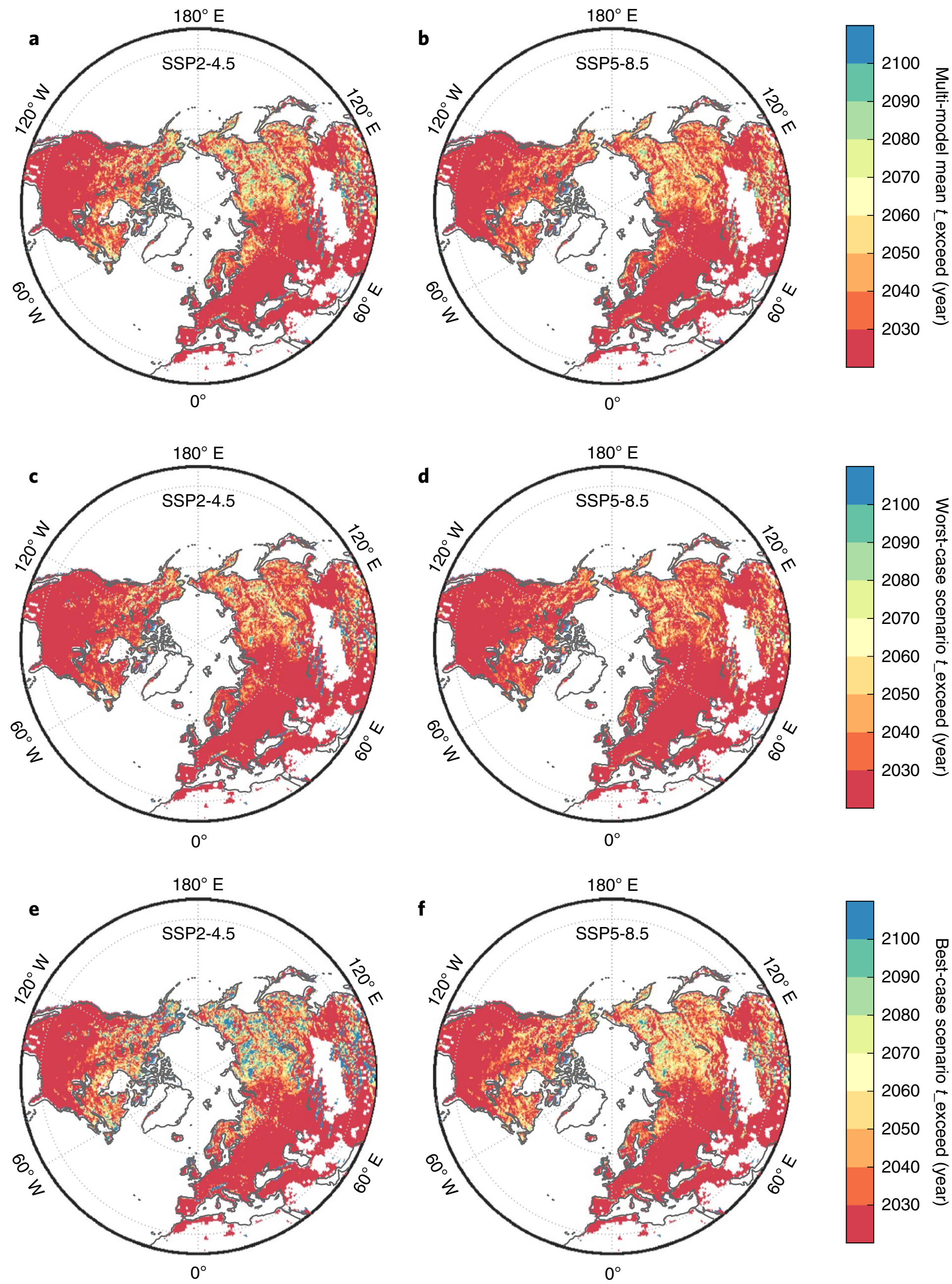

Fig. 3 | Spatiotemporal patterns of the timing (t_{exceed}) when summer temperature exceeds the optimal temperature for vegetation productivity (T_{opt}). **a,b**, Multi-model mean t_{exceed} under SSP2-4.5 (**a**) and SSP5-8.5 (**b**), defined as the timing when model-projected summer temperature first exceeds T_{opt}. **c,d**, The worst-case scenario of multi-model t_{exceed} under SSP2-4.5 (**c**) and SSP5-8.5 (**d**), defined as the earliest 25th percentile across the eight models. **e,f**, The best-case scenario of t_{exceed} under SSP2-4.5 (**e**) and SSP5-8.5 (**f**), defined as the latest 25th percentile across the eight models.

on correlations (from positive to negative) between summer GPP and temperature from ESM simulations and obtained t_{exceed} from observation-based T_{opt}. Under both scenarios, t_{exceed} is much earlier than $t_{negative}$, due to several possible reasons. First, plants can thermally acclimate to climate, so that T_{opt} can change over time with warming[23,24]. The derivative of t_{exceed}, however, may not consider the acclimation of vegetation to warming over time, because the T_{opt} used in our study was derived from historical satellite observations and was assumed to be constant over time. In fact, this thermal acclimation is also evident in the spatial pattern of T_{opt}, because T_{opt} tends to be higher for plants grown in warmer than in colder regions[15,25]. This process of thermal acclimation could also be extended to varying T_{opt} over time, which has been increasingly adopted in current state-of-the-art ESMs[26,27]. For example, the acclimation of photosynthesis to temperature based on mean air temperature has been introduced into the Community Earth System Model for species using the C_3 photosynthesis pathway[26]. The thermal acclimation of T_{opt} in ESMs substantially alleviates the negative impact of future warming, allowing plants to operate at higher temperatures without reducing photosynthesis (GPP)[28]. ESMs with temperature-acclimated T_{opt} could thus lead to a delayed $t_{negative}$ in most of the vegetated land in the NH compared with t_{exceed}, which is derived from a fixed T_{opt}.

Second, enhanced water-use efficiency (WUE) under elevated concentrations of atmospheric CO_2 may also help account for the difference between $t_{negative}$ and t_{exceed}. Both field experiments that manipulate CO_2 levels and large-scale ecosystem analyses have suggested that increases in atmospheric CO_2 levels tend to limit plant transpiration due to partial stomatal closure, hence reducing the amount of water needed for the same amount of photosynthetic fixation of C[29–32]. For example, Keenan et al. reported a significant mean WUE trend of 1.07 ± 3 (mean±standard deviation) gC per $kg\,H_2O\,h\,Pa\,yr^{-1}$ across seven sites in the United States of America over the past two decades[33]. This trend of increasing WUE caused by elevated CO_2 concentration was suggested as the dominant contributor of the increased summer net C uptake for most sites, whereas only a small fraction of the increasing trend was attributed to climatic factors[33]. Spring transpiration savings through higher WUE may also mitigate summer dryness[34], although warming-induced earlier spring may cancel this seasonal teleconnected water-saving effect[35]. These effects can substantially weaken the effect of soil water deficits on plant growth in a warmer future[36], therefore partially offsetting the potential negative impacts of summer warming on photosynthesis. All eight models considered here simulate the CO_2 effect on stomatal conductance, which can suppress transpiration by partial stomatal closure and result in enhanced WUE under elevated CO_2 concentrations (Supplementary Table 1). GPP growth under warming in ESM simulations could thus continue beyond the original T_{opt} derived from historical observations, leading to a delayed $t_{negative}$ compared with t_{exceed} determined using a fixed T_{opt}.

Third, vegetation dynamics could affect the responses of ecosystem productivity to climate change and thus may also contribute to the difference between $t_{negative}$ and t_{exceed}. These processes, usually characterized using dynamic global vegetation models (DGVMs) that simulate vegetation competition, disturbances and climatic feedbacks[37,38], have been included in some but not all ESMs. We evaluated how the inclusion of vegetation dynamics could affect $t_{negative}$ by further dividing the ESMs into two groups based on whether or not they have incorporated DGVMs (Supplementary Table 2). The ESMs with DGVMs generally predicted a later $t_{negative}$ over most of the NH land than those without DGVMs (Supplementary Fig. 10). Interestingly, the difference between the two groups of ESMs under both emission scenarios is mainly in the transitional latitudinal zones, where the effect of warming on plant growth shifts from positive to negative. This phenomenon is probably due to woody encroachment toward higher latitudes, induced by warming that transforms biome composition into biomes adapted to warming in temperature-sensitive regions[37,39]. Multi-model average $t_{negative}$ calculated by the ESMs without DGVMs, however, is notably still much later than t_{exceed}, suggesting that vegetation dynamics may not be the main cause of the delayed $t_{negative}$.

Finally, biases in the structures and parameterization of the ESMs may also have contributed to the difference between $t_{negative}$ and t_{exceed}. The eight ESMs generally identified the pattern of historically observed $R_{GPP-Temp}$ (Supplementary Fig. 11), but the relationship between GPP and temperature is complex and can be influenced by many physiological and environmental factors, particularly soil moisture. Additionally, the output of GPP from the CMIP6 ESMs is at a monthly timescale, which prevents accurate estimation of ESM-based T_{opt} compared with T_{opt} derived from satellite observations with higher resolutions. For improved model evaluations, we recommend that carbon-cycle model outputs be archived at relatively high spatial and temporal resolutions. A global benchmarking of carbon-cycle models against experiments of ecosystem warming is also needed to facilitate model calibration and evaluation.

This study focused on summer, as that is the peak season for plant photosynthesis and warming is most likely to have direct inhibiting effects on vegetation. Nonetheless, we recognize that the annual total GPP also includes carbon uptake in spring and autumn. However, unlike summer, our further analysis suggests that warming consistently enhances spring vegetation productivity for almost the entire NH throughout the twenty-first century under both scenarios (Supplementary Fig. 12a,b), and enhances autumn GPP for most of the NH mid–high latitudes (Supplementary Fig. 12c,d), due to lower spring and autumn temperatures than summer. Productivity in autumn is less responsive to warming than in spring, as GPP in the late growing season is more constrained by solar radiation[40,41] and soil water deficits[42]. Collectively, increases in GPP during these two seasons by warming should partially compensate for the negative effect of above-optimum high temperatures on summer GPP. Thus, $t_{negative}$ is believed to be further delayed when considering the overall productivity of the entire growing season. Despite this, an approaching temperature turning point within this century in the summer is critical for understanding future ecosystem function, vegetation dynamics and carbon balance.

The CMIP6 ESMs predicted that ecosystem GPP will respond negatively to summer warming across most of the extratropical NH vegetated land by the end of this century. Exceptions are the Arctic and the Tibetan Plateau, where plant photosynthesis continues to increase with further summer warming even in the worst-case scenario. Our findings therefore indicated that continuous warming could decrease vegetation productivity and negatively impact the global land carbon sink. We have no reason to be optimistic, even for cold-region ecosystems where the positive effect of warming on GPP could persist throughout the twenty-first century, because few ESMs consider ecological dynamics associated with the degradation of permafrost, such as vegetation successions and biome shifts[7,43]. Such processes can profoundly affect arctic and alpine ecosystems[44]. The incorporation of permafrost degradation and its associated ecological processes into models would thus probably enable a refined re-evaluation of responses of ecosystem productivity to warming in high-latitude and alpine ecosystems. The general trend of warming shifting from increasing to decreasing vegetation productivity in the NH highlights the need for strategies of adaptation and mitigation to minimize future negative impacts on ecosystem functioning induced by ongoing climatic warming.

Online content

Any methods, additional references, Nature Research reporting summaries, source data, extended data, supplementary information, acknowledgements, peer review information; details of author contributions and competing interests; and statements of data and code availability are available at https://doi.org/10.1038/s41558-022-01374-w.

Received: 4 October 2021; Accepted: 26 April 2022;
Published online: 30 May 2022

References

1. Friedlingstein, P. et al. Global carbon budget 2020. *Earth Syst. Sci. Data* **12**, 3269–3340 (2020).
2. Myneni, R. B. et al. A large carbon sink in the woody biomass of northern forests. *Proc. Natl Acad. Sci. USA* **98**, 14784–14789 (2001).
3. Sitch, S. et al. Recent trends and drivers of regional sources and sinks of carbon dioxide. *Biogeosciences* **12**, 653–679 (2015).
4. Kauppi, P. E. et al. Large impacts of climatic warming on growth of boreal forests since 1960. *PLoS ONE* **9**, e111340 (2014).
5. Zhu, Z. C. et al. Greening of the Earth and its drivers. *Nat. Clim. Change* **6**, 791–795 (2016).
6. Piao, S. L. et al. Characteristics, drivers and feedbacks of global greening. *Nat. Rev. Earth Environ.* **1**, 14–27 (2020).
7. IPCC *Climate Change 2013: The Physical Science Basis* (eds Stocker, T. F. et al.) (Cambridge Univ. Press, 2013).
8. Penuelas, J. et al. Shifting from a fertilization-dominated to warming-dominated period. *Nat. Ecol. Evol.* **1**, 1438–1445 (2017).
9. D'Arrigo, R., Wilson, R., Liepert, B. & Cherubini, P. On the 'divergence problem' in northern forests: a review of the tree-ring evidence and possible causes. *Glob. Planet. Change* **60**, 289–305 (2008).
10. Beck, P. S. A. et al. Changes in forest productivity across Alaska consistent with biome shift. *Ecol. Lett.* **14**, 373–379 (2011).

11. Vickers, H. et al. Changes in greening in the High Arctic: insights from a 30-year AVHRR max NDVI dataset for Svalbard. *Environ. Res. Lett.* **11**, 105004 (2016).
12. Piao, S. L. et al. Evidence for a weakening relationship between interannual temperature variability and northern vegetation activity. *Nat. Commun.* **5**, 5018 (2014).
13. Duffy, K. A. et al. How close are we to the temperature tipping point of the terrestrial biosphere? *Sci. Adv.* **7**, eaay1052 (2021).
14. Liu, Y. W. et al. Seasonal responses of terrestrial carbon cycle to climate variations in CMIP5 models: evaluation and projection. *J. Clim.* **30**, 6481–6503 (2017).
15. Huang, M. T. et al. Air temperature optima of vegetation productivity across global biomes. *Nat. Ecol. Evol.* **3**, 772–779 (2019).
16. Park, T. et al. Changes in timing of seasonal peak photosynthetic activity in northern ecosystems. *Glob. Change Biol.* **25**, 2382–2395 (2019).
17. Keeling, C. D., Chin, J. F. S. & Whorf, T. P. Increased activity of northern vegetation inferred from atmospheric CO_2 measurements. *Nature* **382**, 146–149 (1996).
18. Piao, S. L., Friedlingstein, P., Ciais, P., Viovy, N. & Demarty, J. Growing season extension and its impact on terrestrial carbon cycle in the Northern Hemisphere over the past 2 decades. *Glob. Biogeochem. Cycles* **3**, GB3018 (2007).
19. Keenan, T. F. et al. Net carbon uptake has increased through warming-induced changes in temperate forest phenology. *Nat. Clim. Change* **4**, 598–604 (2014).
20. Xia, J. Y. et al. Joint control of terrestrial gross primary productivity by plant phenology and physiology. *Proc. Natl Acad. Sci. USA* **112**, 2788–2793 (2015).
21. Eyring, V. et al. Overview of the Coupled Model Intercomparison Project Phase 6 (CMIP6) experimental design and organization. *Geosci. Model Dev.* **9**, 1937–1958 (2016).
22. Meehl, G. A. & Tebaldi, C. More intense, more frequent, and longer lasting heat waves in the 21st century. *Science* **305**, 994–997 (2004).
23. Yamori, W., Hikosaka, K. & Way, D. A. Temperature response of photosynthesis in C3, C4, and CAM plants: temperature acclimation and temperature adaptation. *Photosynth. Res.* **119**, 101–117 (2014).
24. Berry, J. & Bjorkman, O. Photosynthetic response and adaptation to temperature in higher plants. *Annu. Rev. Plant Physiol. Plant Mol. Biol.* **31**, 491–543 (1980).
25. Chen, A., Huang, L., Liu, Q. & Piao, S. L. Optimal temperature of vegetation productivity and its linkage with climate and elevation on the Tibetan Plateau. *Glob. Change Biol.* **27**, 1942–1951 (2021).
26. Smith, N. G., Lombardozzi, D., Tawfik, A., Bonan, G. & Dukes, J. S. Biophysical consequences of photosynthetic temperature acclimation for climate. *J. Adv. Model. Earth Syst.* **9**, 536–547 (2017).
27. Chen, M. & Zhuang, Q. L. Modelling temperature acclimation effects on the carbon dynamics of forest ecosystems in the conterminous United States. *Tellus B* **65**, 19156 (2013).
28. Crous, K. Y. Plant responses to climate warming: physiological adjustments and implications for plant functioning in a future, warmer world. *Botany* **106**, 1049–1051 (2019).
29. Conley, M. M. et al. CO_2 enrichment increases water-use efficiency in sorghum. *New Phytol.* **151**, 407–412 (2001).
30. Norby, R. J. & Zak, D. R. Ecological lessons from free-air CO_2 enrichment (FACE) experiments. *Annu. Rev. Ecol. Evol. Syst.* **42**, 181–203 (2011).
31. Huang, M. T. et al. Change in terrestrial ecosystem water-use efficiency over the last three decades. *Glob. Change Biol.* **21**, 2366–2378 (2015).
32. Gonsamo, A. et al. Greening drylands despite warming consistent with carbon dioxide fertilization effect. *Glob. Change Biol.* **7**, 3336–3349 (2021).
33. Keenan, T. F. et al. Increase in forest water-use efficiency as atmospheric carbon dioxide concentrations rise. *Nature* **499**, 324–327 (2013).
34. Lemordant, L. et al. Modification of land–atmosphere interactions by CO_2 effects: implications for summer dryness and heat wave amplitude. *Geophys. Res. Lett.* **43**, 10240–10248 (2016).
35. Lian, X. et al. Summer soil drying exacerbated by earlier spring greening of northern vegetation. *Sci. Adv.* **6**, eaax0255 (2020).
36. Lian, X. et al. Multifaceted characteristics of dryland aridity changes in a warming world. *Nat. Rev. Earth Environ.* **4**, 232–250 (2021).
37. Druel, A., Ciais, P., Krinner, G. & Peylin, P. Modeling the vegetation dynamics of northern shrubs and mosses in the ORCHIDEE land surface model. *J. Adv. Model. Earth Syst.* **11**, 2020–2035 (2019).
38. Scheiter, S., Langan, L. & Higgins, S. I. Next-generation dynamic global vegetation models: learning from community ecology. *New Phytol.* **198**, 957–969 (2013).
39. Mod, H. K. & Luoto, M. Arctic shrubification mediates the impacts of warming climate on changes to tundra vegetation. *Environ. Res. Lett.* **12**, 124028 (2016).
40. Zhang, Y., Commane, R., Zhou, S., Williams, A. P. & Gentine, P. Light limitation regulates the response of autumn terrestrial carbon uptake to warming. *Nat. Clim. Change* **10**, 739–743 (2020).
41. Bauerle, W. L. et al. Photoperiodic regulation of the seasonal pattern of photosynthetic capacity and the implications for carbon cycling. *Proc. Natl Acad. Sci. USA* **109**, 8612–8617 (2012).
42. Zhang, Y., Parazoo, N. C., Williams, A. P., Zhou, S. & Gentine, P. Large and projected strengthening moisture limitation on end-of-season photosynthesis. *Proc. Natl Acad. Sci. USA* **117**, 9216–9222 (2020).
43. Fritz, M. et al. Brief communication: future avenues for permafrost science from the perspective of early career researchers. *Cryosphere* **9**, 1715–1720 (2015).
44. Jin, X. Y. et al. Impacts of climate-induced permafrost degradation on vegetation: a review. *Adv. Clim. Change Res.* **12**, 29–47 (2021).

Publisher's note Springer Nature remains neutral with regard to jurisdictional claims in published maps and institutional affiliations.

Methods

Earth system model outputs. We used monthly outputs of GPP, near-surface air temperature (T_{air}), precipitation (Pr), surface downwelling shortwave radiation (Rad) and maximum near-surface air temperature (T_{airmax}) from nine ESMs (Supplementary Table 3) participating in CMIP6 under SSPs 2-4.5 and 5-8.5, which are the only collections available covering 2001–2100. All ESM outputs can be downloaded from the Institute Pierre-Simon Laplace server (https://esgf-node.ipsl.upmc.fr/search/cmip6-ipsl/). Variables for the northern (>23.5° N) vegetated land were bilinearly interpolated to 0.5 × 0.5° in longitude and latitude, subset and aggregated to the summer (June–August) on a yearly timescale.

Reversal time of warming-enhanced vegetation productivity. We first applied partial correlation analysis between annual summer GPP and T_{air} ($R_{GPP–Temp}$; Pr and Rad as the controlling variables) for 2001–2100 for each ESM using a 20-year moving window (from 2001–2020 to 2081–2100). Linear trends were first removed for all variables within each 20-year window and the result was indexed to the final year (for example, $R_{GPP–Temp}$ for 2020 was the correlation between GPP and T_{air} for 2001–2020). We then defined the time at which warming shifts from increasing to decreasing summer vegetation productivity ($t_{negative}$) using $R_{GPP–Temp}$, ranging from 2020 to 2100. For each grid cell, $t_{negative}$ was the year when $R_{GPP–Temp}$ first shifts from positive to significantly negative ($R_{GPP–Temp} < 0$, $P < 0.05$).

We evaluated ESM-based $R_{GPP–Temp}$ against observation-based $R_{GPP–Temp}$ for 2001–2014 to further validate our results. The observation-based $R_{GPP–Temp}$ was calculated using FLUXCOM GPP data[45] and CRU/NCEP-derived climatic data (summer temperature, precipitation and downward shortwave radiation). The ESMs generally identified the pattern of $R_{GPP–Temp}$ using the observation-based results, reinforcing our confidence in the future projections (Supplementary Fig. 11). Note, however, that the modelling results from the medium-resolution version of the Beijing Climate Center Climate System Model (BCC-CSM2-MR) indicated a contrasting $R_{GPP–Temp}$ for northern Eurasia compared with that from observations and other ESMs, suggesting a lack of ability to project $R_{GPP–Temp}$ with accuracy. We thus excluded BCC-CSM2-MR from further analysis, retaining a total of eight ESMs. Moreover, productivity–temperature relationships were also reconstructed between FLUXCOM GPP and temperature and between solar-induced fluorescence[46] and temperature for the period 2001–2015 (2020) to compare with multi-model mean $R_{GPP–Temp}$ at the beginning of this century (Supplementary Fig. 3).

Timing of temperature over optimal-productivity requirement. We used a historically observed optimal temperature for vegetation productivity (T_{opt}) derived from the curve for the response of GPP to temperature using eddy covariance measurements and satellite data from Huang et al.[15]. We compared T_{opt} for each ensemble ESM with the 20-year running average T_{airmax} for 2001–2020 to 2081–2100 (with each 20-year moving window result indexed to its final year) to detect the timing (t_{exceed}) when model-projected maximum summer temperature exceeds T_{opt}. We did not directly use model-projected maximum temperature due to the inherent biases in ESM projections. We instead bias-corrected the projections following a delta method from Navarro-Racines et al.[47]. The relative changes in this delta method between ESM-projected future and recent (2001–2013) summer temperatures were added to the current observed temperatures from CRU/NCEP for each pixel and model to generate future adjusted projections.

Data availability

All data used in this study are openly available from the following: CMIP6 (https://esgf-node.ipsl.upmc.fr/search/cmip6-ipsl/); FLUXCOM GPP (http://fluxcom.org/CF-Download/); contiguous solar-induced fluorescence (https://osf.io/8xqy6/); CRU/NCEP temperature (https://dataguru.lu.se/app) and T_{opt} (Huang et al[15]; https://www.nature.com/articles/s41559-019-0838-x). Any additional information may be obtained from the corresponding author upon reasonable request.

Code availability

All computer codes used in this study are available via GitHub at https://github.com/minimiminiminimiffy/Productivity-Temperature.

References

45. Tramontana, G. et al. Predicting carbon dioxide and energy fluxes across global FLUXNET sites with regression algorithms. *Biogeosciences* **13**, 4291–4313 (2016).
46. Zhang, Y., Joiner, J., Alemohammad, S. H., Zhou, S. & Gentine, P. A global spatially contiguous solar-induced fluorescence (CSIF) dataset using neural networks. *Biogeosciences* **15**, 5779–5800 (2018).
47. Navarro-Racines, C., Tarapues, J., Thornton, P., Jarvis, A. & Ramirez-Villegas, J. High-resolution and bias-corrected CMIP5 projections for climate change impact assessments. *Sci. Data* **7**, 7 (2020).

Acknowledgements

This study was supported by the National Natural Science Foundation of China (41988101) and the Second Tibetan Plateau Scientific Expedition and Research programme (grant no. 2019QZKK0405). A.C. acknowledges the support from a US Department of Energy grant (DE-SC0022074). B.M.R. thanks support from the National Aeronautics and Space Administration (NASA) Arctic-Boreal Vulnerability Experiment (ABoVE) and Carbon Cycle Science programs (NNX17AE13G) and the Gordon and Betty Moore Foundation (grant #8414).

Author contributions

S.P. designed the research, Y.Z. performed the analysis and drafted the figures, Y.Z. and S.P. wrote the first draft of the manuscript and all authors contributed to the interpretation of the results and to the text.

Competing interests

The authors declare no competing interests.

Additional information

Supplementary information The online version contains supplementary material available at https://doi.org/10.1038/s41558-022-01374-w.

Correspondence and requests for materials should be addressed to Shilong Piao.

Peer review information *Nature Climate Change* thanks Alexander Koch and Sassan Saatchi for their contribution to the peer review of this work.